Atmospheric Environment 276 (2022) 119032

Contents lists available at ScienceDirect

Atmospheric Environment

journal homepage: www.elsevier.com/locate/atmosenv

Simulating tropospheric BrO in the Arctic using an artificial neural network

Ilias Bougoudis [a,*], Anne-Marlene Blechschmidt [a], Andreas Richter [a], Sora Seo [a,b], John P. Burrows [a]

[a] Institute of Environmental Physics, University of Bremen, Bremen, 28359, Germany
[b] German Aerospace Center (DLR), Oberpfaffenhofen, 82234, Germany

HIGHLIGHTS

- The prediction of BrO plumes is required to assess the loss of tropospheric ozone
- We present an artificial neural network, which simulates Arctic tropospheric BrO
- The neural network reproduces spatial patterns of many tropospheric BrO plumes
- The trend reported in the observations is not evident in the simulations

ARTICLE INFO

Keywords:
Artificial neural network
Atmospheric chemistry
Bromine explosion
Ozone depletion
Arctic

ABSTRACT

An intriguing natural phenomenon occurs every polar spring, namely the bromine explosion, in which plumes of tropospheric bromine monoxide (BrO) are formed. These plumes are observed in the BrO vertical column densities (VCDs), retrieved from satellite sensors. Tropospheric BrO depletes tropospheric ozone and facilitates the deposition of mercury. Bromine molecules are mainly released from young sea ice, and meteorological parameters determine the formation and evolution of enhanced BrO VCD plumes. Due to the complexity of the physicochemical processes involved in the bromine explosion, the modeling of tropospheric BrO VCDs in chemical transport models is challenging and not yet adequate. The first of its type, this study demonstrates the potential of using an artificial neural network (ANN), which uses meteorological parameters and sea ice age as inputs to simulate and predict tropospheric BrO VCDs in the Arctic. The ANN is trained and validated using a 22-year satellite remote sensing dataset of Arctic tropospheric BrO VCDs. A generally satisfactory spatial agreement between observed and simulated tropospheric BrO VCDs is observed. However, the magnitude of the observed BrO VCD plumes is underestimated. Air temperature and mean sea level pressure are the most important parameters influencing the magnitude of tropospheric BrO VCD simulations. Although the changing spatial distribution of tropospheric BrO VCDs over time is well captured, the trend reported in the observations of tropospheric BrO VCDs is not reproduced by the ANN, suggesting that additional parameters not included in the ANN also influence the formation of tropospheric BrO VCD plumes.

1. Introduction

Human activities are warming the Earth (IPCC, 2021). However, the Arctic is warming more rapidly than the mid-latitudes, a phenomenon known as Arctic Amplification (Serreze and Barry, 2011). During spring in the sunlit Arctic, tropospheric ozone (O_3) depletion occurs (Barrie et al., 1988). These events are associated with elevated concentrations of bromine monoxide (BrO), formed in bromine explosions (Barrie and Platt, 1997). In recent years, the spatial patterns of Arctic BrO plumes have been reported to be changing in the period of Arctic Amplification (Bougoudis et al., 2020).

BrO is an atmospheric free radical formed by the reaction of bromine with O_3 and plays an important role in stratospheric and tropospheric chemistry. Changes in magnitude and distribution of tropospheric BrO lead to changes in O_3 and thus in the oxidizing capacity of the atmosphere, as the most important tropospheric oxidizing agent, the hydroxyl radical, OH, is generated from the photolysis of O_3. Since the discovery of tropospheric O_3 depletion events, several studies have

* Corresponding author. ,
E-mail address: ibougoudis@iup.physik.uni-bremen.de (I. Bougoudis).

https://doi.org/10.1016/j.atmosenv.2022.119032
Received 20 October 2021; Received in revised form 24 February 2022; Accepted 26 February 2022
Available online 1 March 2022

investigated bromine explosions, using observations from campaigns (e.g., Roscoe et al., 2014; Toohey et al., 1990; Tuckermann et al., 1997) satellite remote sensing (e.g., Platt and Wagner, 1998; Richter et al., 1998; Seo et al., 2019) and ground-based remote sensing (e.g., Kreher et al., 1997; Van Roozendael et al., 2002). Bromine also reacts with and oxidizes elemental mercury, enhancing its deposition, particularly in the Arctic troposphere (Lu et al., 2001 and references therein).

The exact triggering mechanism for bromine explosions is not yet fully understood (Jones et al., 2009). Several studies have investigated the surface and atmospheric conditions during which tropospheric BrO plumes are formed. Young sea ice (Simpson et al., 2007; Wagner et al., 2001), cold liquid brine and frost flowers occurring under conditions of low temperatures (Kaleschke et al., 2004; Sander et al., 2006), blowing snow (Lieb-Lappen and Obbard, 2015), low wind speeds (Jones et al., 2009) and high wind speeds (Blechschmidt et al., 2016) are identified as conditions required for the formation of BrO plumes. Low temperatures enhance the sea-salt fractionation on sea ice, and thereby the existence of bromine and chlorine anions on the surface or in liquid or quasi-liquid layers result in the release of bromine molecules (Br_2) and bromine chloride (BrCl) in the polar atmosphere via complex and non-linear heterogeneous and photochemical reactions (Koop et al., 2000; Hara et al., 2020). The relationship between meteorological conditions and BrO plumes, showing that enhanced BrO forms under apparently contradictory meteorological conditions (e.g., both low and high wind speeds), was investigated by Jones et al. (2009). Seo et al. (2020) investigated correlations between meteorological parameters and the total BrO columns retrieved from satellite measurements. These studies show that the relationship between BrO plumes and the dominant physicochemical parameters is complex and non-linear.

As many parameters play a role in generating bromine explosions and non-linear photochemically initiated autocatalytic cycles are involved, the accurate modeling of tropospheric BrO plumes and the quantitative assessment of the consequences for the tropospheric composition are challenging (Fan and Jacob, 1992; Simpson et al., 2007). Yang et al. (2020) used a chemistry-transport and a chemistry-climate model with a parameterization for blowing snow and compared the resulting BrO fields with GOME-2 satellite retrieved columns and ground-based measurements. They reported correlation coefficients of daily means between 0.1 and 0.71, while the total number of days investigated ranged from 33 to 117 for each case. Huang et al. (2020) simulated the impact of sea salt aerosols from blowing snow on tropospheric BrO using the GEOS-Chem chemical transport model and compared the modeled tropospheric BrO to retrievals from OMI and GOME-2A. They reported daily and monthly correlation coefficients between 0.22 and 0.85. They analyzed a period of three years (i.e., 2007 to 2009), and they applied a threshold of tropospheric BrO VCDs above 5.1×10^{13} molec/cm^2 to the GEOS-Chem simulations for their comparisons. Fernandez et al. (2019) developed the first implementation of polar halogen chemistry for the CAM-chemistry model, providing four years (2007–2011) of polar spring comparisons between GOME-2A and modeling results. They reported normalized mean errors between 0.5 and 2.0 for the differences between model and observations. However, they did not focus on spatial and temporal modeling of satellite observed tropospheric BrO VCDs. Instead, they provided a statistical validation of surface and satellite halogen observations. Herrmann et al. (2021) developed 3D time-dependent simulations of BrO in the Weather Research and Forecasting model coupled with chemistry (WRF-Chem) and compared the simulations to GOME-2A satellite observations. They reported correlations of more than 0.6 at Utqiagvik but an under-prediction of modeled BrO VCDs over land and an over-prediction of modeled BrO VCDs over first-year ice. The extensive range of correlation coefficients indicates that a qualitative agreement was found in all studies, but the modeling of bromine explosions is not yet adequate to assess the impact of bromine explosions plumes or accurately project how this will change as global warming increases. The above stimulated our efforts to find an approach to resolve this issue.

Machine learning approaches, particularly neural networks, have often been applied to simulate non-linear problems (Zurada, 1992). Applications of the use of neural networks in atmospheric research include weather prediction (Rasp and Lerch, 2018), remote sensing (Blackwell and Chen, 2005; Müller et al., 2002), ozone forecasting (Comrie, 1997), air quality (Hooyberghs et al., 2005) and OH modeling (Nicely et al., 2020).

Here, we present the first artificial neural network (ANN) to our knowledge to simulate BrO plumes in the Arctic troposphere resulting from bromine explosions. The ANN uses meteorological parameters and sea ice age as inputs to predict the spatial distribution of satellite-derived tropospheric BrO vertical column densities (VCDs). This method is computationally efficient. We propose that this ANN is used as a parameterization tool to initiate BrO VCD plumes in chemical transport models and forecast BrO VCD plumes for measurement campaigns. It also predicts the spatial evolution of enhanced BrO VCD plumes in the warming Arctic. Finally, the degree to which such an ANN can reproduce observations provides insight into the drivers of bromine explosion events.

2. Data and methods

The datasets used in this study are satellite observations of tropospheric BrO VCDs, satellite retrieved sea ice age, and meteorological parameters taken from numerical models. All data were gridded in 0.125 x 0.125 resolution. In addition, this study focuses explicitly on polar spring, as it is the season when bromine explosions most frequently occur.

2.1. Satellite observations of tropospheric BrO VCDs

The Arctic tropospheric BrO VCDs dataset is described in detail in Bougoudis et al. (2020). It comprises a 22-year consolidated dataset (1996–2017) for sea ice-covered regions northwards of 70 N, derived from four UV-VIS satellite sensors. The Slant Column Density (SCD) retrieval was performed using the Differential Optical Absorption Spectroscopy (DOAS) method (Platt and Perner, 1983; Burrows et al., 2011). The total BrO VCD is retrieved by dividing the BrO SCD with a simple stratospheric air mass factor (AMF), calculated by the forward radiative transfer model SCIATRAN (Rozanov et al., 2005). The latter simulates the stratospheric light path and considers the scattering at the surface and in the atmosphere, but not the dependence of the tropospheric light path on observation geometry and surface reflectance. Consequently, the total BrO VCD differs from the sum of the tropospheric and stratospheric columns (Bougoudis et al., 2020). The method proposed by Theys et al. (2009) was used to extract the tropospheric BrO component from the total VCDs. A tropospheric AMF was used in that step, which considers a surface reflectivity of 0.9. Overlapping satellite observations from the same days have been merged by averaging the corresponding grid scenes. The merged tropospheric BrO dataset was validated for consistency during the periods of overlapping measurements by different sensors (Bougoudis et al., 2020). Potential effects due to different instrumental attributes were shown to have a minimum contribution to the geophysical conclusions extracted.

2.2. Sea ice age and meteorological data

The 22-year sea ice age dataset used in the present study is described by Tschudi et al. (2019). It is retrieved from different passive microwave satellite remote sensing instruments and has a very high spatial resolution of 12.5×12.5 km^2, while its temporal sampling is every seven days. It was spatially and temporally interpolated to match the location and time of the satellite observations. In the present study, the presence of sea ice is a prerequisite for estimating bromine explosions.

ECMWF ERA-5 (Hersbach et al., 2018) reanalysis data has been used as meteorological inputs for the ANN. 2 m air temperature, mean sea

level pressure (mslp), 10 m wind speed, 10 m wind direction, and boundary layer height are selected as the key meteorological parameters. They are available for time-steps of 3 h at a spatial resolution of 0.25 . They were interpolated spatially and temporally to each satellite ground scene and observation time.

2.3. Selection of the optimal ANN

ANNs are computing systems inspired by biological neural networks similar to those in the human brain (Wang, 2003). They provide a mathematical representation of the human mind. An ANN comprises many independent processing units (neurons) connected by synapses. The latter are the weights, i.e., the strength of the connection between two neurons. ANNs are structured typically in three layers: the input layer (i.e., the set of independent parameters), the hidden layer (i.e., where the connections between the input and the output layer are performed to interpret complex systems), and the output layer (i.e., the set of dependent parameters we want to model). More complex ANNs may have more than one hidden layer. An ANN acquires knowledge through training. The outputs are calculated by providing a particular set of inputs to the ANN, together with the quantity we want to model (targets). Some of the many advantages of ANNs are that they extract hidden knowledge from highly complex data, either by supervised or unsupervised learning and are generally a fast approach (Zurada, 1992). The selection of an adequate learning dataset and an optimal architecture for the ANN, comprising the number of hidden neurons, determines the accuracy of its output.

This study used a simple shallow cascade forward ANN architecture (Warsito et al., 2018). This type of ANN is similar to feed-forward networks (i.e., the input layer is connected to the hidden, and then the hidden to the output layer) but includes an additional connection from the input and every previous layer to the following layers. In the case of one hidden layer, the output layer is also connected directly with the input layer, besides with the hidden layer. The main advantage of this type of ANN is that it exploits the non-linear relationship between inputs and targets without neglecting the linear relationship between the two (Warsito et al., 2018). The number of hidden neurons was set to 30. A strict formula for selecting the optimal number of hidden neurons does not exist, but many empirical rules are applied (Masters, 1993; Sthathakis, 2009), considering the number of input parameters and instances. If the number of neurons is too large, the ANN will adapt its weights to the current training data and not perform accurate predictions on different datasets. If the number of neurons is too small, it will lead to over-simplification and make the ANN incapable of exploiting hidden relationships between inputs and targets.

In this study, and considering the amount of training data (i.e., approximately 1 million grid scenes per year), the number of hidden neurons selected provides a combination of efficiency and simplicity. We have tested the results for selected daily ANN simulations of tropospheric BrO VCDs (outputs) for different numbers of neurons. Using a larger number of hidden neurons did not improve the results, whereas using a smaller number decreased the accuracy of the outputs. The reduction in complexity resulted in the ANN being incapable of mapping the relationship between inputs and targets. The settings selected in this study provide a fast and accurate approach. The ANN is computationally efficient and has low demands in processing resources. Fig. 1 shows a schematic of the neural network implemented in this study to simulate tropospheric BrO VCDs.

Satellite observed tropospheric BrO VCDs were selected as the quantity we want to model. Sea ice age, 2 m air temperature, mean sea level pressure, 10 m wind speed, boundary layer height, and 10 m wind direction were selected as inputs. They were identified as key parameters associated with bromine explosion events and the production of tropospheric BrO plumes. We assume that the input parameters selected constrain the non-linear physicochemical mechanism, which produces the outputs, sufficiently. No additional spatial (e.g., latitude or longitude) or temporal information is used as input. In this way, the ANN establishes the relationships between the key parameters (inputs) and the observed tropospheric BrO VCDs (targets) without spatial and temporal information interference. In order to identify the best learning dataset, 22 individual ANNs were created. An ANN was trained for each year of data with the corresponding daily data of the year in question (approximately 1 million grid scenes per year). The learning dataset is randomly split into three datasets: 70% into the training dataset, 15%

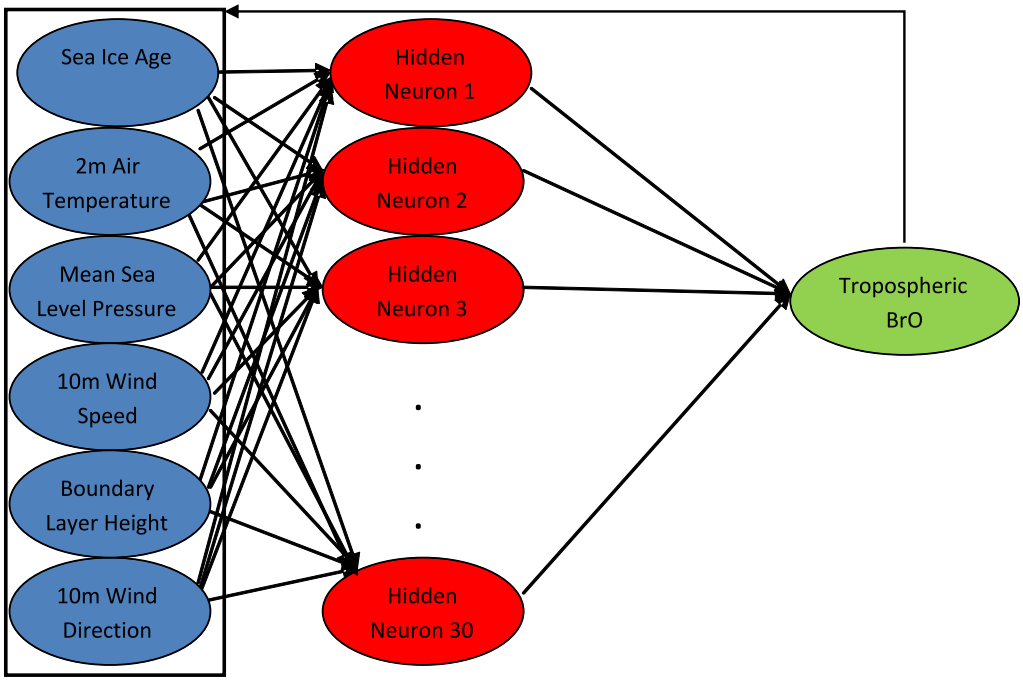

Fig. 1. A schematic of the neural network used in this study. Blue color denotes the input parameters, red color the hidden layer, and green color the neural network's output. The line connecting the output with the inputs denotes the cascade architecture of the ANN. (For interpretation of the references to color in this figure legend, the reader is referred to the Web version of this article.)

into the validation dataset, and 15% into the testing dataset.

The training dataset is used to accurately adjust the weighting factors of each input in order to obtain a close approximation of the target. It computes the gradient and updates the network weights. The validation dataset provides an unbiased evaluation of the fit on the training dataset. The error of the validation dataset is monitored during the training process. It usually decreases during the training process, as does the error of the training dataset. When the network begins to overfit data, the error of the validation dataset begins to rise. Thus, the validation dataset is used to determine an appropriate stopping training point. In this way, over-fitting is avoided, and the ANN becomes more flexible in adapting to new datasets. The testing dataset is used to evaluate the performance of the ANN by comparing targets and outputs without re-adjusting the weighting factors. After the learning process is complete (i.e., training, validation, and testing), the ANN can simulate tropospheric BrO VCDs from other input datasets (years). The metric used to identify the best learning dataset is the annual correlation coefficient between targets and outputs (Fig. 3a). After that step, the best 1-year ANN (i.e., the ANN trained with data from 2007, as shown in Fig. 3a) was chosen to simulate the entire dataset of tropospheric BrO VCDs.

3. Results and discussion

3.1. Relationships between observations of tropospheric BrO VCDs and the input parameters

Fig. 2 shows scatter plots where the ordinate is observations of tropospheric BrO VCDs, for spring (i.e., March, April, and May, MAM), from 1996 to 2017, and the following parameters are the abscissa: sea ice age, 2 m air temperature, mslp, 10 m wind speed and boundary layer height. Each point is a daily average.

The salinity of sea ice decreases as it ages (Kaleschke et al., 2004). Thus the correlation of sea ice age with tropospheric BrO VCDs has a negative sign (i.e., −0.34). Most days with enhanced tropospheric BrO VCDs (i.e., above 5.0×10^{13} molec/cm^2) occur over first-year ice. Some days with tropospheric BrO VCDs above 5.0×10^{13} molec/cm^2 occur over multi-year sea ice, especially over two years old ice. The contribution of multi-year sea ice to the formation of enhanced tropospheric BrO is reported in the literature (Peterson et al., 2019). The days with average sea ice age greater than two and tropospheric BrO VCDs above 5.0×10^{13} molec/cm^2 are rare. A strong anti-correlation between tropospheric BrO VCDs and 2 m air temperature can be observed in Fig. 2b (correlation coefficient of −0.54). All days with tropospheric BrO VCDs above 5.0×10^{13} molec/cm^2 coincide with average daily temperatures below 260 K. These results agree with previous studies (Hara et al., 2020; Sander et al., 2006). Mslp does not correlate strongly with tropospheric BrO VCDs, having a correlation coefficient of −0.12. A reason for this low correlation may be that both low and high-pressure systems contribute to the formation of enhanced tropospheric BrO VCDs (Salawitch et al., 2010; Choi et al., 2012). 10 m wind speed has a weak positive correlation with tropospheric BrO VCDs (i.e., a correlation coefficient of +0.27). The reason may be similar to that of mslp, as both high and low wind speeds favor the appearance of high tropospheric BrO VCDs (Jones et al., 2009). An anti-correlation (i.e., a correlation coefficient of −0.36) between tropospheric BrO VCDs and boundary layer height is shown in Fig. 2e. This is not in agreement with similar literature studies (Choi et al., 2012). For almost all days having tropospheric BrO VCDs above 5.0×10^{13} molec/cm^2, the average boundary layer height was below 500 m. As the scatter plots in Fig. 2 contain daily averages, slightly different results from previous similar studies can be expected. Hidden indirect correlations occur because the quantities discussed here correlate and interact with each other non-linearly. For example, in Fig. 2b, sea ice, especially first-year ice, which is thin, melts and finally disappears as temperature increases. This implies that the decrease observed in tropospheric BrO VCDs with increasing temperature is also a result of a decrease in first-year sea ice extent. Nevertheless, Fig. 2 provides a valuable initial correlation analysis between tropospheric BrO VCDs and the key parameters selected in this study.

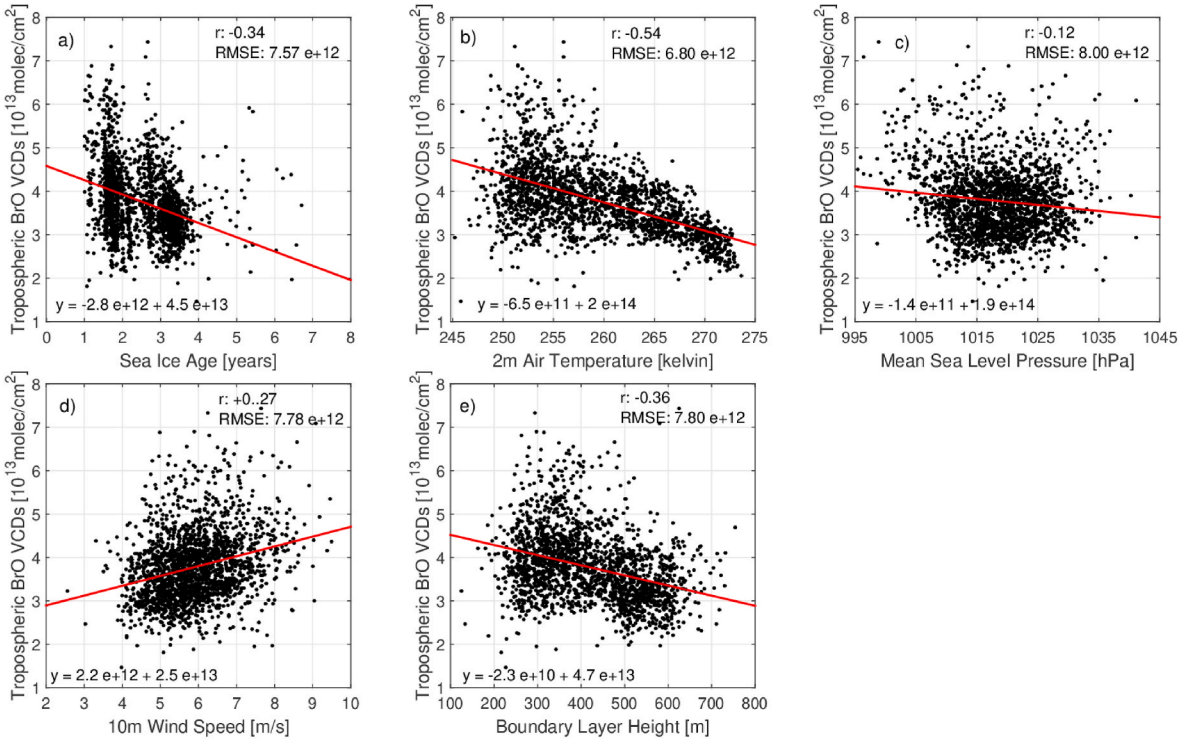

Fig. 2. Daily MAM scatter plots between observed tropospheric BrO VCDs and: a) sea ice age, b) 2 m air temperature, c) Mslp, d) 10 m wind speed, and e) boundary layer height. The best-fitting line, its formula, the correlation coefficient, and the root mean square error between the line and the points are shown in all scatter plots. The period is from 1996 to 2017.

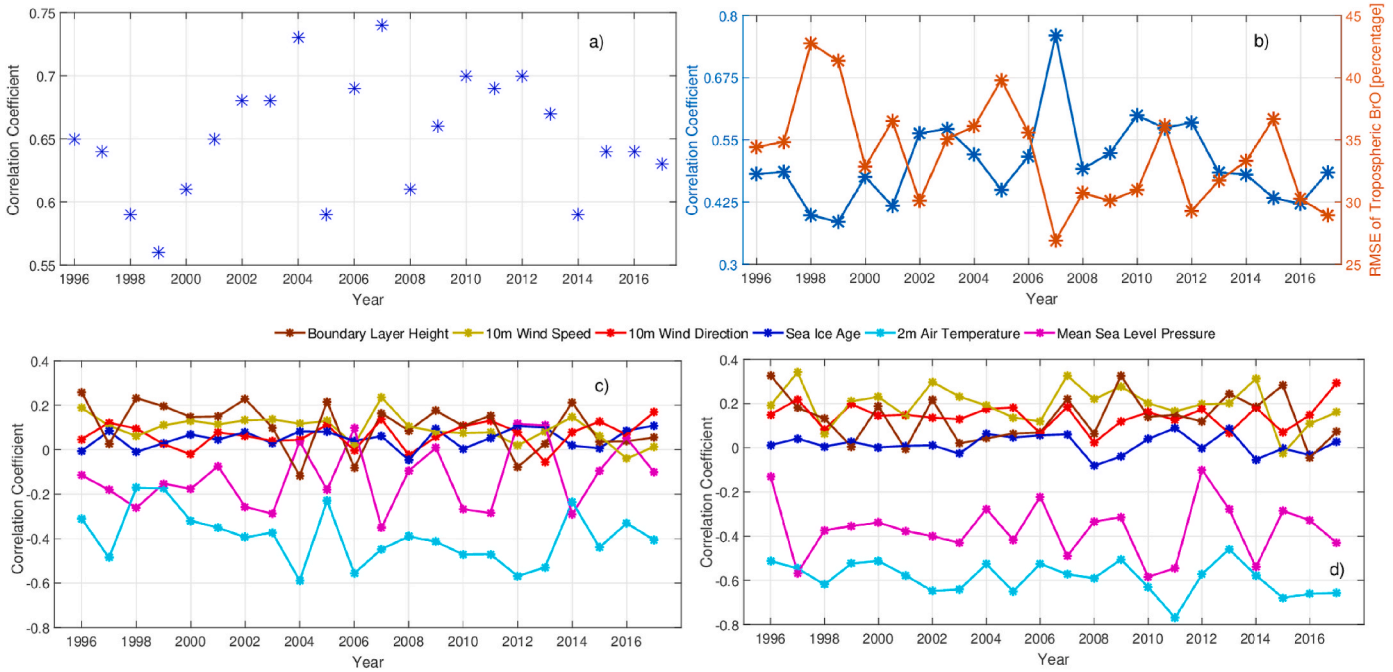

Fig. 3. Plots of the correlation coefficients between the observed tropospheric BrO VCDs, those simulated by the ANN, and the input parameters for the MAM period of each year: a) Correlation coefficients between targets and outputs for the 22 ANNs, b) Correlation coefficients and root mean square errors (RMSE) between observations and simulations produced by the ANN trained with data from 2007, c) Correlation coefficients between observations and inputs, d) Correlation coefficients between simulations and inputs.

3.2. Qualitative assessment of the ANNs

Fig. 3 provides information to assess the performance of the 22 ANNs (Fig. 3a), the comparison between observed tropospheric BrO VCDs (observations) and simulated tropospheric BrO VCDs (simulations) produced by the best ANN (Fig. 3b), the relationships between inputs and observations (Fig. 3c) and the relationships between inputs and simulations (Fig. 3d). All time-series use MAM periods. All metrics (i.e., correlation coefficients and root mean square errors) are calculated using the corresponding grid cells of each year for the quantities of interest, without performing any averaging, in contrast to Fig. 2. Thus, spatial information is considered for the correlation coefficients, and the root mean square errors.

Fig. 3a plots the correlation coefficients between targets (i.e., all the gridded cells of satellite observed tropospheric BrO VCDs) and outputs for each of the 22 ANNs during the training processes. The correlation coefficients are in the range of 0.55–0.75. The ANN trained with 2007 data achieves the highest correlation. This ANN was selected to simulate the entire dataset of observations, as shown in all the following figures. The observations for 2007 have also been discussed in Begoin et al. (2010). Enhanced BrO plumes have been observed in the Arctic and were correlated with low temperatures, high wind speeds, and low-pressure systems.

Fig. 3b shows the reconstruction performance of the whole dataset of observations generated using the 2007 ANN. The analysis was performed for all the daily grid boxes of the MAM periods. The RMSEs are presented as a percentage of the observations. Satisfactory agreement (correlation coefficients of 0.4 or better and root mean square errors on the order of 35%) is found between observations and simulations. A higher correlation coefficient and smaller root mean square error for 2007 are expected because the ANN was trained with this year's observations.

Fig. 3c shows the correlation between the six inputs and observations. Although the input parameters correlate with tropospheric BrO VCDs and each other, these linear correlations (i.e., in Fig. 3c and d) provide a simple relationship between inputs and tropospheric BrO VCDs. The 2 m air temperature and mslp correlate negatively with the observations (correlation coefficients being around −0.4 for the 2 m temperature, −0.2 for mslp). Boundary layer height has the highest positive correlation with the observations (correlation coefficients being approximately +0.15). The second highest positive correlation coefficient is the 10 m wind speed. Sea ice age and 10 m wind direction are weakly correlated with the observations (between +0.2 and 0). Similar findings were reported in Seo et al. (2020) but for total BrO VCDs. The correlations between observations and each input parameter vary significantly between the years (for example, in 2014, mslp has an even higher negative correlation than temperature, while the correlation is approximately 0 in 2009). Similarly, a substantial decrease in the correlation between boundary layer height and observations is seen in 2004.

The same analysis as in Fig. 3c but between inputs and simulations is shown in Fig. 3d. Comparison of Fig. 3c and d shows that the observations and simulations are similarly correlated to the inputs. 2 m air temperature and mslp are negatively correlated (on the order of −0.6 for the simulations for temperature and −0.4 for mslp). 10 m wind speed and boundary layer height are positively correlated (on the order of +0.2 for the simulations), while sea ice age and wind direction show weak positive correlations. This indicates that the selected ANN trained with data from 2007 has reasonably captured the relationships between the inputs and observations. The differences between the correlation coefficients between inputs and simulations compared to those between inputs and observations (especially for 2 m air temperature and mslp) probably indicate the existence of additional parameters, which contribute to the production of observed tropospheric BrO VCDs. The stronger dependence of simulations on these two parameters may also result from the meteorological conditions that occurred in 2007, which was used as the training dataset (e.g., low air temperatures and low-pressure systems that contributed to the formation of enhanced tropospheric BrO VCD plumes). Tables 1 and 2 in the supplementary material provide the correlation coefficients for each year for Fig. 3c and d, respectively.

3.3. Exemplary simulations of bromine explosion events

In late March and early April of 2011, a bromine explosion was observed in the Arctic, linked to cyclone activity. This bromine explosion case and its link to meteorology were investigated thoroughly in Blechschmidt et al. (2016). In Fig. 4, the simulation map for the April 1, 2011 is presented and compared to the observation map and the sea ice age and meteorological conditions of that day.

The comparison of the maps of observations and simulations indicates that the spatial extent of the large BrO VCD plume over the Beaufort Sea is well represented by the ANN. The same applies to the smaller BrO VCD plumes over East Siberian and the Kara Sea. This is a remarkable result considering that the ANN was trained with data from another year, and the input comprised only meteorological and sea ice age data. However, the simulations are smaller in magnitude than the observations (Fig. 4c). Sea ice age, being relatively static, does not provide any meaningful information regarding the plumes. According to Blechschmidt et al. (2016), the bromine explosion event was associated with frontal lifting by a polar cyclone, in agreement with the spatial patterns of meteorological parameters (high wind speeds, low pressure, low temperature, high boundary layer) shown in Fig. 4. The ANN correctly attributes such distinct spatial patterns of meteorological parameters to tropospheric bromine explosions. Similar successful spatial reproductions of observations are found in every year.

However, the neural network does not always spatially identify and reproduce enhanced tropospheric BrO VCD plumes. Such a case is found on the April 8, 2017, shown in Fig. 5.

In the observations, an enhanced tropospheric BrO VCD plume extends from the East Siberian Sea to the Arctic Ocean (Fig. 5a). The neural network could not predict this BrO VCD plume (Fig. 5b). This can also be seen from the difference between observations and simulations (Fig. 5c). By examining sea ice age and meteorological parameters on that day, a high mslp over the region where the enhanced tropospheric BrO VCD was observed is found (i.e., around 1020 hPa, Fig. 5f). This value is much higher than the one observed over the tropospheric BrO VCD plume on April 01, 2011 (i.e., 982 hPa, Fig. 4f). 2 m air temperature was also higher than on April 01, 2011 (257 K in Fig. 5d, compared to 248 K in Fig. 4d).

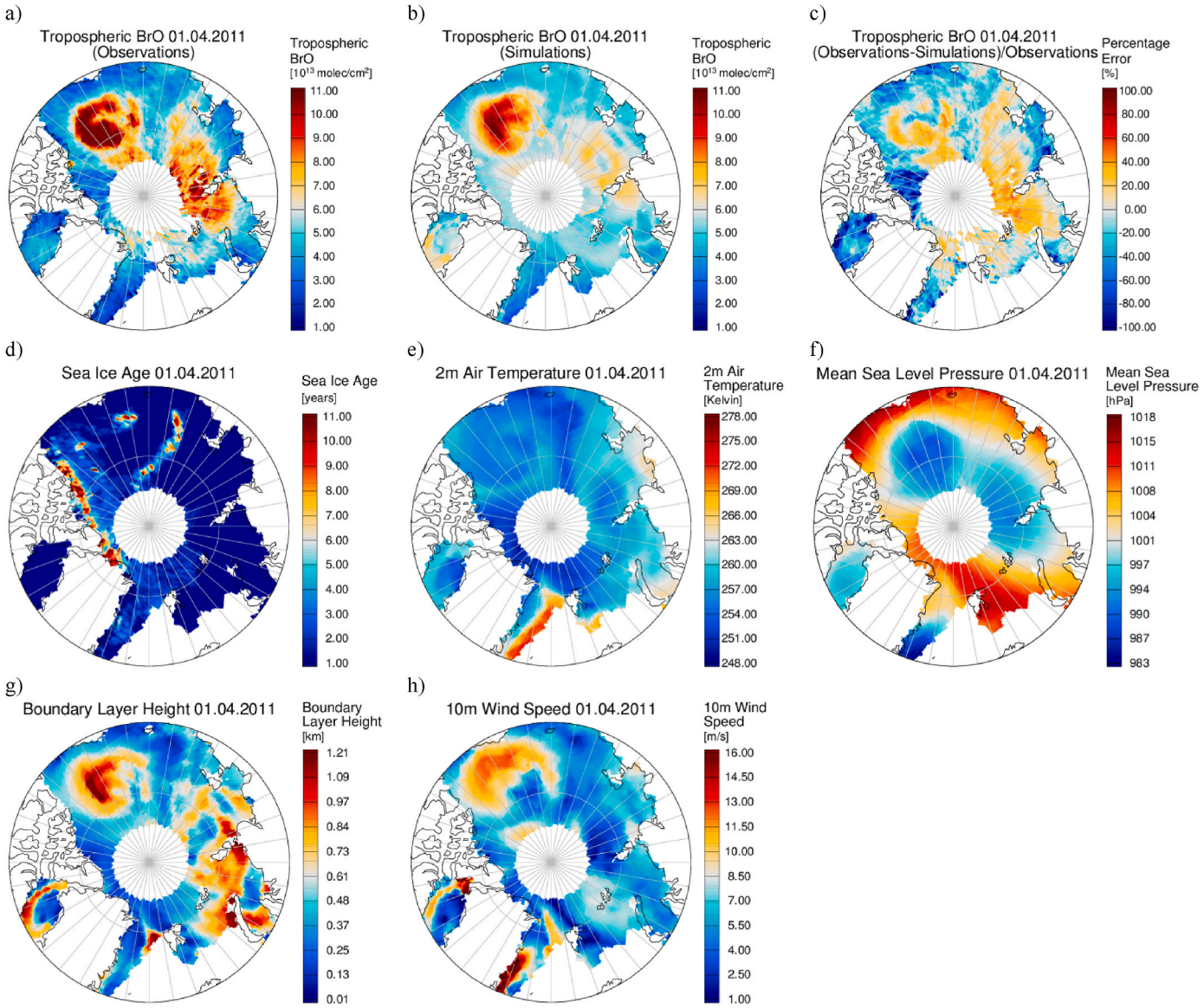

Fig. 4. Daily polar plots of observations, simulations, relative differences between them, and inputs for a bromine explosion event on April 01, 2011 a) observations, b) simulations, c) relative differences between observations and simulations (i.e., (observations-simulations)/observations), d) sea ice age, e) 2 m air temperature, f) mslp, g) boundary layer height, h) 10 m wind speed.

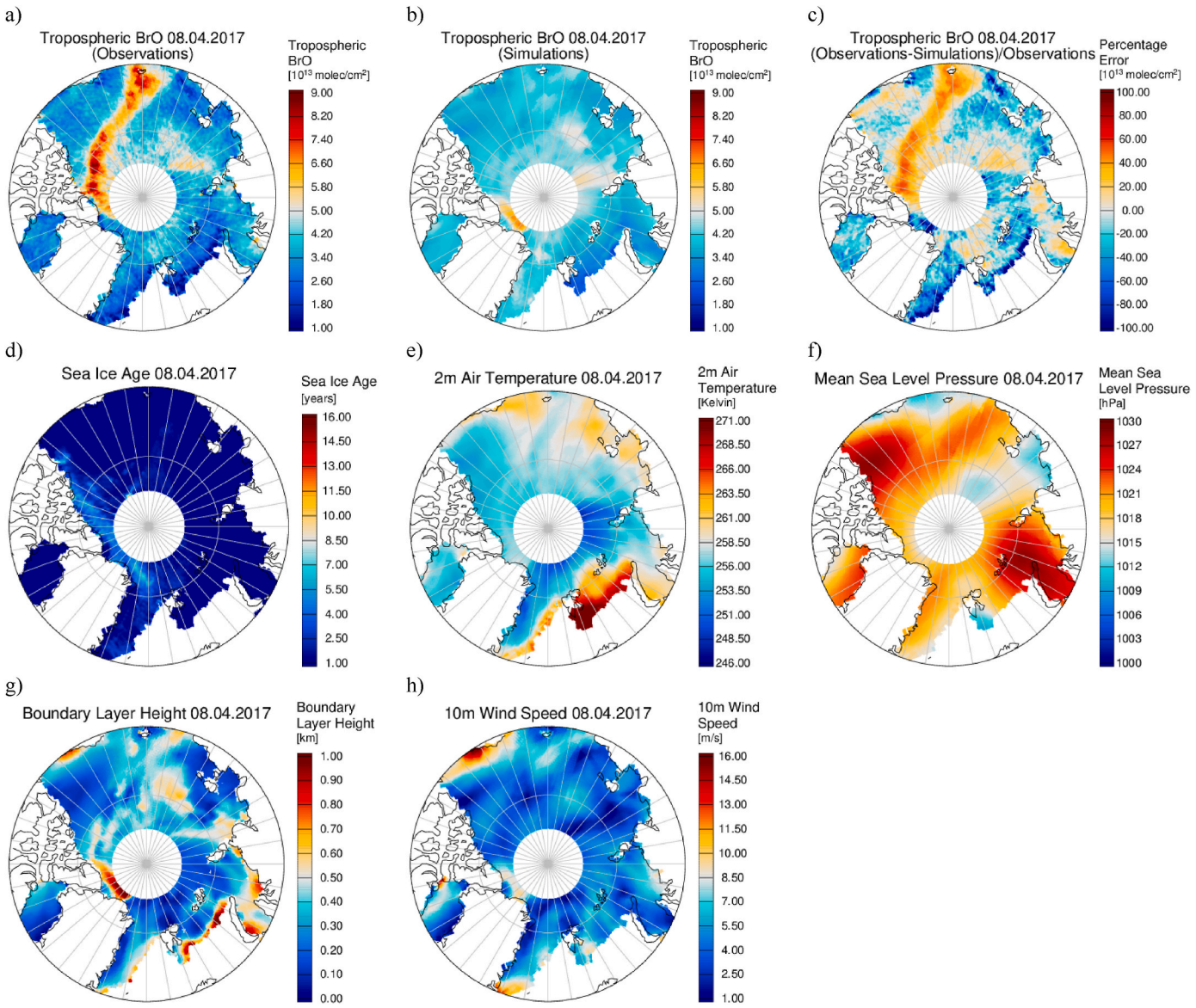

Fig. 5. Daily polar plots of observations, simulations, relative differences between them, and inputs for a bromine explosion event on April 08, 2017 a) observations, b) simulations, c) relative differences between observations and simulations (i.e., (observations-simulations)/observations), d) sea ice age, e) 2 m air temperature, f) mslp, g) boundary layer height, h) 10 m wind speed.

Salawitch et al. (2010) suggested that high satellite-derived BrO VCDs can be the product of stratospheric air extending to lower altitudes above high-pressure surface systems. As the observations do not provide the vertical distribution of BrO (i.e., the altitude of the plume), plumes that occur at higher altitudes are not directly related to the surface parameters chosen as inputs to the neural network and cannot be spatially reproduced by it. Differences between observations and simulations can be attributed to geophysical processes and parameters not included in this study (e.g., the occurrence of blowing snow and sea-salt aerosols, which can transport and recycle bromine molecules far away from their initial release site). Similar results occur for the April 8, 2017, even by training the neural network with 2017 data. Such days appear in every year of the dataset. A discussion on the potential reasons for the differences observed in such days follows in section 3.6.

3.4. Impact of meteorology and sea ice age on the magnitude of the simulations

A limited sensitivity analysis has been undertaken to investigate the impact of each input parameter on the simulations' magnitude. The values of the selected input parameter varied over the range of the daily mean values of the 22-year dataset, while all other input parameters were kept constant at their 2007 mean MAM value. The simulations were then plotted as a function of the selected input parameter (Fig. 6).

The maximum simulated tropospheric BrO VCD occurs over first-year ice. We attribute this to the higher salinity of first-year ice (Jacobi et al., 2006). This impact on the magnitude of the simulations is not as important as that of the change of 2 m air temperature. A rapid decrease of the simulations from 9.0×10^{13} molec/cm^2 to 5.0×10^{13} molec/cm^2 occurs as 2 m air temperature increases from 240 K to 247 K. Above 247 K, the magnitude of the simulations continues to decrease, after a small increase around 250 K, but with a smaller gradient. Seo et al. (2020), Kaleschke et al. (2004), and Frieß et al. (2011) reported that bromine explosions often occur at temperatures below 250 K, consistent with Sander et al. (2006) and the sensitivity tests reported in this study. Although the ANN does not consider any information on parameters, which have been identified to influence bromine release at low temperatures, such as liquid brine, carbonate precipitation (Sander

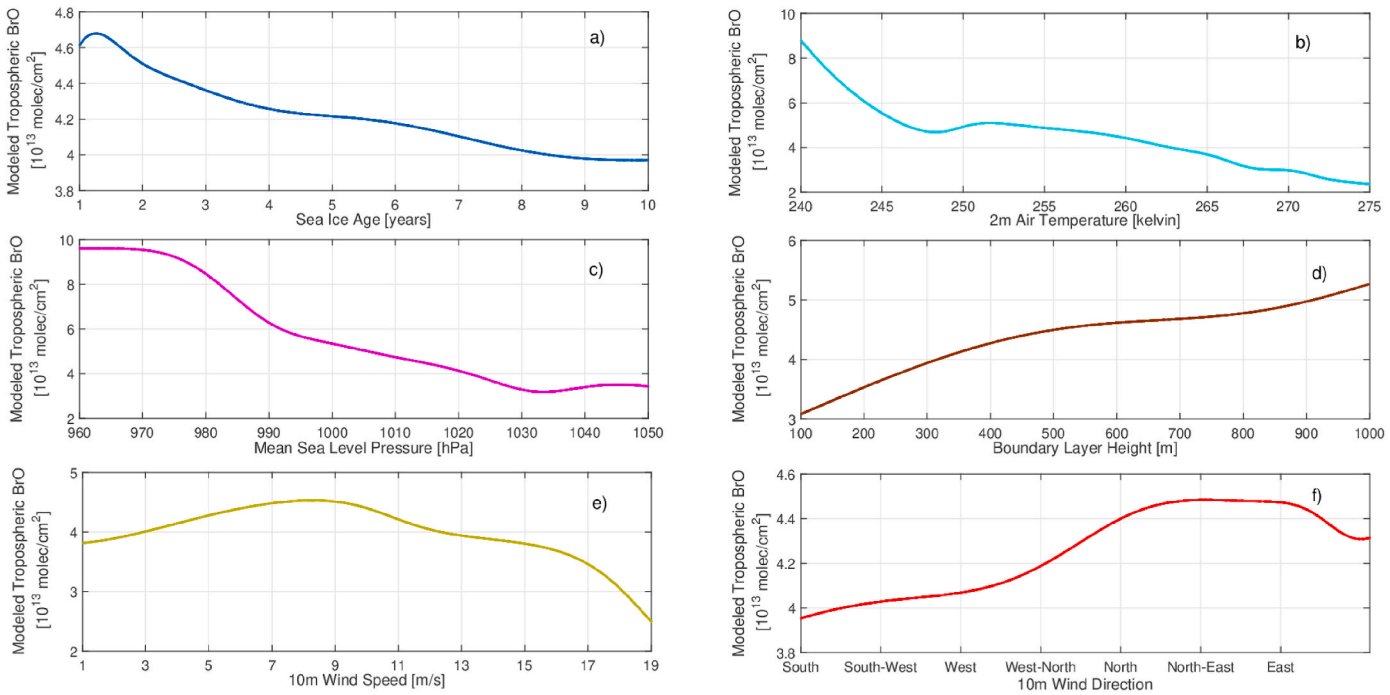

Fig. 6. Simulated BrO VCDs plotted as a function of a) sea ice age, b) 2 m air temperature, c) mslp, d) boundary layer height, e) 10 m wind speed, and f) 10 m wind direction. In each case, all other input parameters are set to the MAM average value of 2007.

et al., 2006), or sea salt fractionation on sea ice (Hara et al., 2020), it still identifies the relationship between enhanced tropospheric BrO VCDs and low temperatures.

Mslp also has a significant impact on the magnitude of the simulations. Several studies reported that low-pressure systems favor the formation of tropospheric BrO VCD plumes (Seo et al., 2020; Jones et al., 2010). Choi et al. (2012) and Blechschmidt et al. (2016) reported that low-pressure systems, coupled with a high boundary layer and high wind speeds, favor the formation of tropospheric BrO VCD plumes. Similar meteorological conditions also occurred during the training period of 2007 and resulted in the bromine explosion event described by Begoin et al. (2010). This contributed to the strong sensitivity of the simulations to mslp. The positive correlation between boundary layer height and simulations is explained using the same reasoning.

A surprising relationship between 10 m wind speed and simulations was found. A positive correlation can be observed up to 9 m/s, followed by a negative correlation for wind speeds above this value. This is in contrast to other studies suggesting that high wind speeds contribute to the formation of enhanced tropospheric BrO VCD plumes (Blechschmidt et al., 2016; Jones et al., 2009). The reason for this may be that the enhancement of tropospheric BrO through heterogeneous reactions occurring on blowing snow and sea-salt aerosols, which can be released from sea ice surfaces under the presence of strong winds (Hara et al., 2018; Frey et al., 2020) is not accounted for in the ANN. The 10 m wind speed impact on the simulations does not appear to be as pronounced as that of 2 m air temperature and mslp. The air mass may be more rapidly diluted at higher wind speeds. In addition, all other meteorological parameters are kept at their 2007 MAM mean values, which may not be realistic for high wind speeds.

The highest magnitude of the simulations occurs with the wind blowing from the North, North-East, and East direction, as cold air masses are transported from sea ice regions. Seo et al. (2020) reported that the highest total BrO VCDs were observed at northerly and north-westerly winds. However, the sensitivity of the simulations to wind direction is comparatively small.

3.5. Long-term comparisons between observations and simulations

In Fig. 7, mean MAM maps of observations and simulations are compared from 1996 to 2017.

These mean maps show that the largest observed tropospheric BrO VCDs in the region of the East Siberian Sea occurred between 1996 and 2004. 2004 is the first year that enhanced observations are identified over the Beaufort Sea. Until 2009, the simulations are spatially in good agreement with the observations. For almost all years (i.e., 1999 is the only exception), the regions of enhanced observations are reproduced successfully by the ANN simulations. A decrease in performance of the ANN can be seen from 2009 onwards. In 2009, multi-year ice extent decreased significantly, giving its place to first-year ice (Bougoudis et al., 2020). Since that year, the observations indicate that the number of bromine explosions has increased, and they may appear over almost the entire Arctic region. The annual mean values of mslp usually show high pressure over the Beaufort Sea (Serreze and Barrett, 2010). The simulations could not reproduce the enhanced observations in this region for some years (e.g., 2009, 2013, and 2015). It is inferred from Fig. 3c that in 2009 the correlation coefficient between mslp and observations was almost 0 and continued to be insignificant over the following years. This might also explain the decline of the performance of the ANN from 2009 onwards. This is unclear but may imply that the temperatures are not as low in the low-pressure regions as previously. Thus the non-linearity of the bromine explosion mechanism and its dependence on the physicochemical behavior of the cryosphere require additional constraints for the ANN to predict more accurately the tropospheric BrO VCDs under all conditions.

Fig. 8 plots the mean MAM time-series for observations and simulations of tropospheric BrO VCDs. The 1σ error bars are also plotted for the observations.

Bougoudis et al. (2020) reported an increasing trend in spring observations over the Arctic from 1996 to 2017 of 1.5% per year, with an error of 0.2% per year. The mean ANN simulated BrO VCDs agree reasonably well with the observed when considering the errors in the observations. However, the identified positive trend is not evident in the simulations, as they are higher than the observations from 1996 to 2003

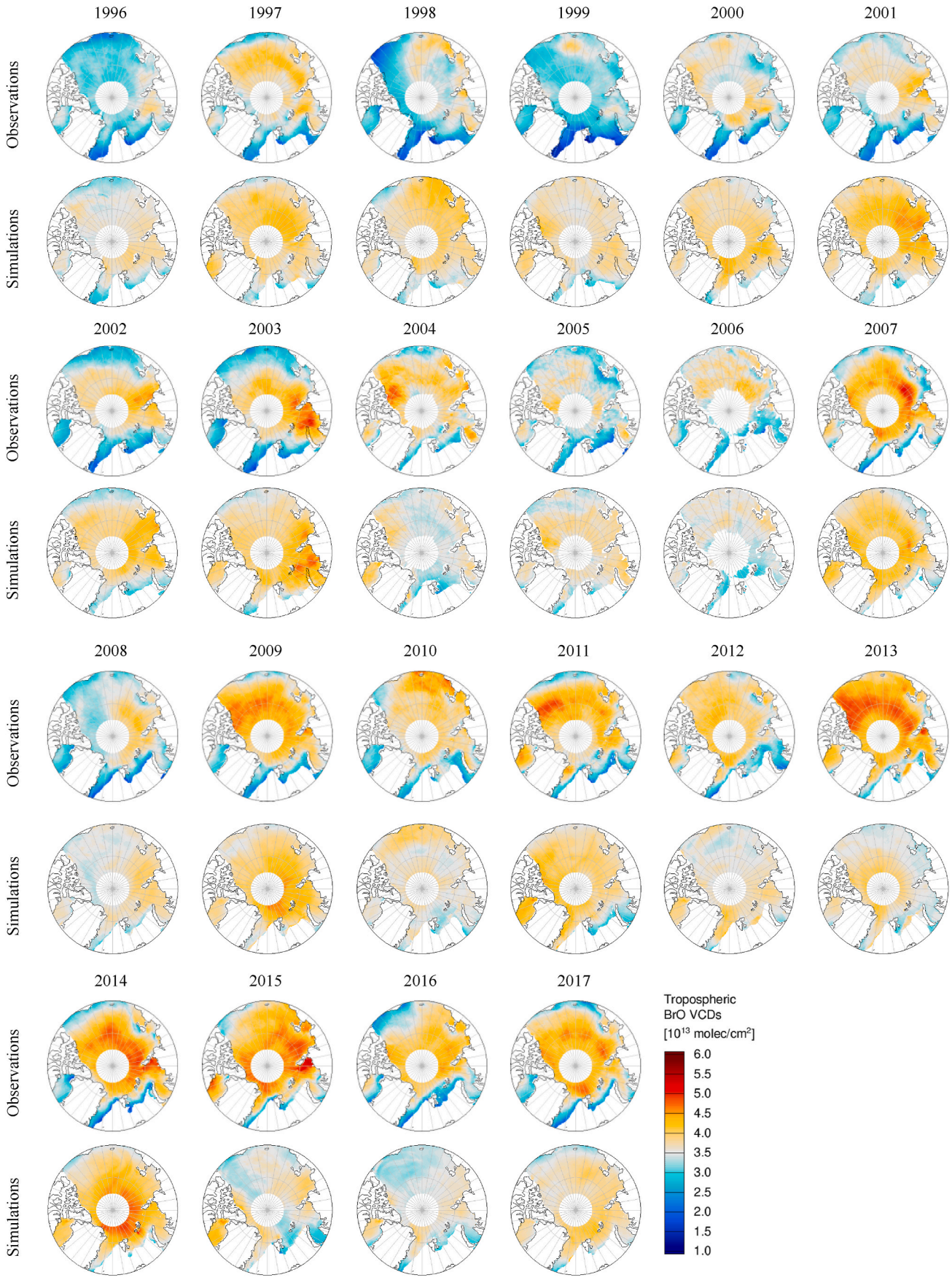

Fig. 7. Comparisons of Arctic tropospheric BrO VCDs MAM maps between observations and simulations. Columns indicate years, odd-numbered rows the observations, and even-numbered rows the simulations.

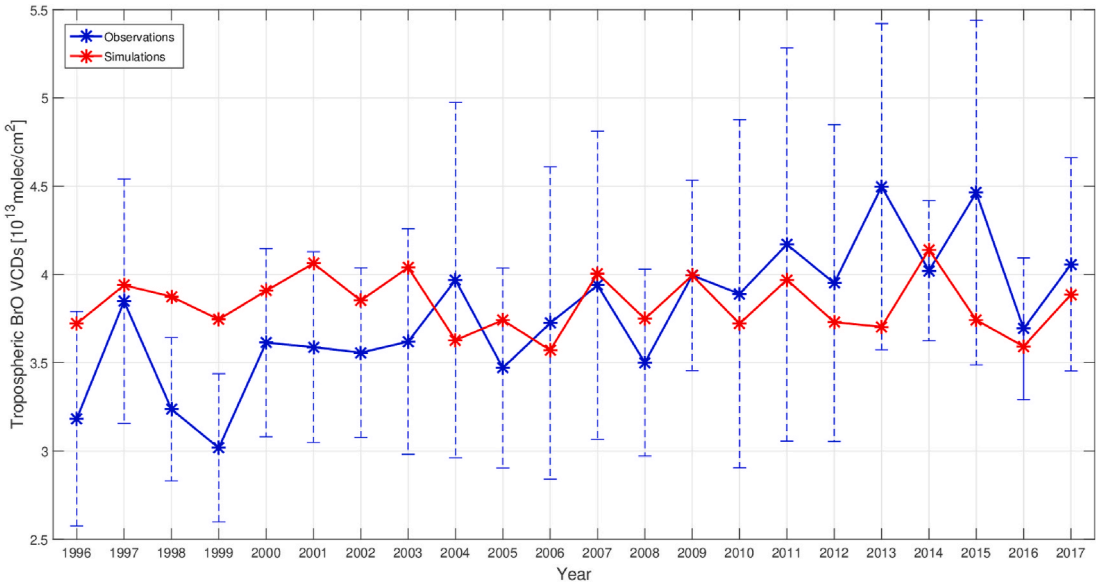

Fig. 8. Mean MAM time-series of BrO VCD observations and simulations.

and lower from 2010 to 2017. The main strength of the neural network is the spatial reproduction of daily enhanced tropospheric BrO plumes. From days similar to April 01, 2011 (i.e., Fig. 4), the magnitude of the enhanced tropospheric BrO modeled by the neural network is also acceptable. The differences between observations and simulations are considerable for days similar to the one in Fig. 5 (i.e., April 07, 2017), especially over high-pressure systems. Such differences may cause the deviations that we see in Fig. 8. The agreement in the time-series does not necessarily verify the successful spatial reproduction of enhanced tropospheric BrO plumes. For example, in 2009 and 2014, the averaged simulated MAM value is similar to the observed MAM average. However, the comparison of the corresponding maps in Fig. 7 shows poor spatial agreement for these two years.

3.6. Discussion

In the following, we discuss some additional parameters that may improve the ANN's accuracy. The best explanation for the absence of the trend in the ANN simulated BrO VCDs may be that some tropospheric BrO sources are not influenced by changes in the inputs currently used in the ANN. This indicates that other parameters than those considered thus far also impact the formation of enhanced tropospheric BrO VCD plumes.

Aerosol, cloud, snow, or ice particles covered with sufficient brine are known to play an important role in the heterogeneous chemistry of the bromine explosions (Choi et al., 2018; Hara et al., 2018; Frey et al., 2020). The transport of aerosol and snow from snowpack by strong winds can result in brine being transported, enabling bromine explosions to generate BrO VCD plumes potentially far from their source region (Peterson et al., 2017). Observations of suitable aerosol optical thickness are not yet available for potential use in the ANN. Although wind speed is used as input, this bromine source mechanism may require additional parameters, which better constrain this behavior, to simulate tropospheric BrO VCDs more accurately. Potential contribution that is at a distance from the ignition location of the surface bromine source is not yet addressed by the ANN input parameters.

Tropospheric BrO VCDs can be vertically lifted above the boundary layer (Blechschmidt et al., 2016; Frieß et al., 2011; Peterson et al., 2017). This limits the VCD-based modeling approach presented here. We consider that including the vertical profile of tropospheric BrO plumes would resolve this limitation. However, as yet, relevant observations of the vertical profile of BrO in the Arctic do not exist in sufficient numbers.

We note that bromine explosions are only observed under illuminated conditions. For this study, the variation of solar irradiation was not considered explicitly in the ANN input. A sufficient actinic flux of solar radiation photolyzing Br_2 and BrCl is a prerequisite for bromine explosions. However, the mechanism is an autocatalytic physicochemical chain reaction and thus most likely has no strong dependence on the initial amount of Br once an actinic flux above a threshold is achieved. In addition, there are no suitable actinic flux data available yet to extend the ANN input.

Finally, it is worth noting that when comparing observations to aircraft measurements, Choi et al. (2012) found that stratospheric variability substantially influences the total BrO VCD, with its magnitude being comparable to the magnitude of the tropospheric signal. Thus, errors in the separation of the stratospheric and tropospheric BrO VCDs in the satellite data may influence the performance of the ANN.

4. Summary and conclusions

This paper presents a machine learning approach using an ANN to simulate Arctic tropospheric BrO VCD plumes formed during bromine explosions. These events are challenging to model in chemistry transport or chemistry-climate models. They are important because of their impact on tropospheric O_3 and mercury and thus on tropospheric pollution and indirectly on climate change. This is the first study of its type and demonstrates the strengths and weaknesses of the ANN approach to simulate tropospheric BrO VCDs.

The selection of an adequate set of inputs for the ANN is required to model tropospheric BrO VCDs successfully. In this ANN, the following inputs were used: sea ice age, 2 m air temperature, mean sea level pressure, 10 m wind speed, 10 m wind direction, and the boundary layer height. The 22-year tropospheric BrO VCD dataset, retrieved from satellite remote sensing by Bougoudis et al. (2020), was used for training and quality assessment of the ANN. The evaluation of the ANN setups for different years showed that the ANN trained with data from 2007 was the most successful. It was then selected and used to simulate the tropospheric BrO VCDs for all the years between 1996 and 2017.

This ANN reproduces well the spatial extent of the tropospheric BrO VCD plumes from those bromine explosions, which typically occur in low-pressure systems under low air temperatures and high boundary layer conditions. Therefore, it is not surprising that mslp and 2 m air temperature seem to be the most sensitive parameters for the magnitude of the simulations. Although data-driven and unaware of

physicochemical processes that trigger bromine explosions, the ANN identifies hidden links and relationships between tropospheric BrO VCDs and the input parameters used.

The comparisons between observations and simulations during the available 22 MAM seasons show a satisfactory spatial agreement between observed and simulated tropospheric BrO VCDs up to 2009 but a small underestimation in more recent years. There are some bromine explosions cases where the ANN underestimates the observed tropospheric BrO VCDs. These tropospheric BrO VCD plumes typically occur at higher latitudes and do not strongly correlate with the input surface parameters. This indicates that the observed changes in bromine explosion events are not driven solely by changes in the parameters used as inputs for the ANN, which are typically at or close to the surface.

The current inability of the ANN to predict specific types of bromine explosions and the trend in the observations is attributed to missing information content (e.g., the vertical distribution of tropospheric BrO VCD, cyclone tracks, aerosol optical depth, snow coverage, liquid brine, sea salt fractionation on sea ice) in the current ANN input. By including temporal and spatial parameters together with detailed vertical information, the ANN could recognize BrO plumes' evolution (e.g., bromine emissions in one place, deposition in another, and later re-emission to the atmosphere at different altitudes).

The ANN approach presented in this study to estimate tropospheric BrO VCD plumes is different from previous studies, which used atmospheric chemistry models as it is data-driven. It provides a fast and computationally low-cost solution to simulate tropospheric BrO VCDs during periods of bromine explosions. Although other modeling studies reported higher correlation coefficients in some cases (e.g., Herrmann et al., 2021), the level of spatial agreement between observations and simulations achieved by the ANN is higher than that of traditional modeling approaches.

Overall, the ANN is a robust and fast approach to model tropospheric BrO VCDs using meteorological and sea ice data. It can be used for future short and medium-scale projections of the spatial distribution of tropospheric BrO plumes. The current ANN can be used as a fast and straightforward parameterization tool to predict tropospheric BrO VCDs for the planning purposes of future measurement campaigns. In addition, it can be coupled to chemical transport models or chemistry-climate models for studies on the impact of bromine explosions on the tropospheric oxidizing capacity and indirect impacts or feedback on climate change.

Author contributions

I. Bougoudis collected and processed the meteorological data, performed the analysis, and prepared the paper. J.P. Burrows and A.-M Blechschmidt initiated this study. The research presented was supervised by A.-M. Blechscmidt, A. Richter and J.P. Burrows. A. Richter developed software that was used for plotting BrO data. All authors contributed to the writing of the paper.

Data availability

Part of the tropospheric BrO VCD data of this study is available through the World Data Center PANGAEA (https://doi.pangaea.de/10.1594/PANGAEA.906046). The EASE-Grid Sea ice age version 4 was provided by NSIDC from their website (https://nsidc.org/data/nsidc-0611/versions/4). Hersbach, H. et al. (2018) was downloaded from the Copernicus Climate Change Service (C3S) Climate Data Store. The results contain modified Copernicus Climate Change Service information 2020. Neither the European Commission nor ECMWF is responsible for any use that may be made of the Copernicus information or data it contains. Matlab software was used in this study. The data and method to produce the results are available upon request from the corresponding author.

Declaration of competing interest

The authors declare that they have no known competing financial interests or personal relationships that could have appeared to influence the work reported in this paper.

Acknowledgments

We gratefully acknowledge the funding by the Deutsche Forschungsgemeinschaft (DFG, German Research Foundation) - Projektnummer 268020496 – TRR 172, within the Transregional Collaborative Research Center "ArctiC Amplification: Climate Relevant Atmospheric and SurfaCe Processes, and Feedback Mechanisms (AC)^{3}" and the University of Bremen.

Appendix A. Supplementary data

Supplementary data related to this article can be found online at https://doi.org/10.1016/j.atmosenv.2022.119032

References

Barrie, L.A., Bottenheim, J.W., Schnell, R.C., Crutzen, P.J., Rasmussen, R.A., 1988. Ozone destruction and photochemical reactions at polar sunrise in the lower Arctic atmosphere. Nature 334, 138–141. https://doi.org/10.1038/334138a0.

Barrie, L., Platt, U., 1997. Arctic tropospheric chemistry: an overview. Tellus B 49, 450–454. https://doi.org/10.1034/j.1600-0889.49.issue5.2.x.

Begoin, M., Richter, A., Weber, M., Kaleschke, L., Tian-Kunze, X., Stohl, A., Theys, N., Burrows, J.P., 2010. Satellite observations of long range transport of a large BrO plume in the Arctic. Atmos. Chem. Phys. 10, 6515–6526. https://doi.org/10.5194/acp-10-6515-2010.

Blackwell, W.J., Chen, F.W.-M., 2005. Neural Network Applications in High-Resolution Atmospheric Remote Sensing. https://archive.ll.mit.edu/publications/journal/pdf/vol15_no2/15_2-09.pdf.

Blechschmidt, A.-M., Richter, A., Burrows, J.P., Kaleschke, L., Strong, K., Theys, N., Weber, M., Zhao, X., Zien, A., 2016. An exemplary case of a bromine explosion event linked to cyclone development in the Arctic. Atmos. Chem. Phys. 16, 1773–1788. https://doi.org/10.5194/acp-16-1773-2016.

Bougoudis, I., Blechschmidt, A.-M., Richter, A., Seo, S., Burrows, J.P., Theys, N., Rinke, A., 2020. Long-term time-series of arctic tropospheric BrO derived from UV-VIS satellite remote sensing and its relation to first year sea ice. Atmos. Chem. Phys. 20, 11869–11892. https://doi.org/10.5194/acp-20-11869-2020.

Burrows, J.P., Borrell, P., Platt, U., 2011. In: The remote sensing of tropospheric composition from space,. springer Berlin Heidelberg, Berlin, Heidelberg. https://doi.org/10.1007/978-3-642-14791-3_1.

Choi, S., Theys, N., Salawitch, R.J., Wales, P.A., Joiner, J., Canty, T.P., Chance, K., Suleiman, R.M., Palm, S.P., Cullather, R.I., Darmenov, A.S., Silva, A. da, Kurosu, T. P., Hendrick, F., Roozendael, M.V., 2018. Link between arctic tropospheric BrO explosion observed from space and sea-salt aerosols from blowing snow investigated using ozone monitoring instrument BrO data and GEOS-5 data assimilation system. J. Geophys. Res. Atmos. 123, 6954–6983. https://doi.org/10.1029/2017JD026889.

Choi, S., Wang, Y., Salawitch, R.J., Canty, T., Joiner, J., Zeng, T., Kurosu, T.P., Chance, K., Richter, A., Huey, L.G., Liao, J., Neuman, J.A., Nowak, J.B., Dibb, J.E., Weinheimer, A.J., Diskin, G., Ryerson, T.B., Silva, A. da, Curry, J., Kinnison, D., Tilmes, S., Levelt, P.F., 2012. Analysis of satellite-derived Arctic tropospheric BrO columns in conjunction with aircraft measurements during ARCTAS and ARCPAC. Atmos. Chem. Phys. 12, 1255–1285. https://doi.org/10.5194/acp-12-1255-2012.

Comrie, A.C., 1997. Comparing neural networks and regression models for ozone forecasting. J. Air Waste Manag. Assoc. 47, 653–663. https://doi.org/10.1080/10473289.1997.10463925.

Fan, S.-M., Jacob, D.J., 1992. Surface ozone depletion in Arctic spring sustained by bromine reactions on aerosols. Nature 359, 522–524. https://doi.org/10.1038/359522a0.

Fernandez, R.P., Carmona-Balea, A., Cuevas, C.A., Barrera, J.A., Kinnison, D.E., Lamarque, J.-F., Blaszczak-Boxe, C., Kim, K., Choi, W., Hay, T., Blechschmidt, A.-M., Schönhardt, A., Burrows, J.P., Saiz-Lopez, A., 2019. Modeling the sources and chemistry of polar tropospheric halogens (Cl, Br, and I) using the CAM-chem global chemistry-climate model. J. Adv. Model. Earth Syst. 11, 2259–2289. https://doi.org/10.1029/2019MS001655.

Frey, M.M., Norris, S.J., Brooks, I.M., Anderson, P.S., Nishimura, K., Yang, X., Jones, A. E., Nerentorp Mastromonaco, M.G., Jones, D.H., Wolff, E.W., 2020. First direct observation of sea salt aerosol production from blowing snow above sea ice. Atmos. Chem. Phys. 20, 2549–2578. https://doi.org/10.5194/acp-20-2549-2020.

Frieß, U., Sihler, H., Sander, R., Pöhler, D., Yilmaz, S., Platt, U., 2011. The vertical distribution of BrO and aerosols in the Arctic: measurements by active and passive differential optical absorption spectroscopy. J. Geophys. Res. Atmos. 116 https://doi.org/10.1029/2011JD015938.

Hara, K., Osada, K., Yabuki, M., Matoba, S., Hirabayashi, M., Fujita, S., Nakazawa, F., Yamanouchi, T., 2020. Atmospheric sea-salt and halogen cycles in the Antarctic.

Environ. Sci.: Process. Impact 22, 2003–2022. https://doi.org/10.1039/D0EM00092B.
Hara, K., Osada, K., Yabuki, M., Takashima, H., Theys, N., Yamanouchi, T., 2018. Important contributions of sea-salt aerosols to atmospheric bromine cycle in the Antarctic coasts. Sci. Rep. 8, 1–8. https://doi.org/10.1038/s41598-018-32287-4.
Herrmann, M., Sihler, H., Frieß, U., Wagner, T., Platt, U., Gutheil, E., 2021. Time-dependent 3D simulations of tropospheric ozone depletion events in the Arctic spring using the Weather Research and Forecasting model coupled with Chemistry. Atmos. Chem. Phys. 21, 7611–7638. https://doi.org/10.5194/acp-21-7611-2021.
Hersbach, H., Bell, B., Berrisford, P., Hirahara, S., Horányi, A., Muñoz-Sabater, J., Nicolas, J., Peubey, C., Radu, R., Schepers, D., Simmons, A., Soci, C., Abdalla, S., Abellan, X., Balsamo, G., Bechtold, P., Biavati, G., Bidlot, J., Bonavita, M., Chiara, G. D., Dahlgren, P., Dee, D., Diamantakis, M., Dragani, R., Flemming, J., Forbes, R., Fuentes, M., Geer, A., Haimberger, L., Healy, S., Hogan, R.J., Hólm, E., Janisková, M., Keeley, S., Laloyaux, P., Lopez, P., Lupu, C., Radnoti, G., Rosnay, P. de, Rozum, I., Vamborg, F., Villaume, S., Thépaut, J.-N., 2018. The ERA5 Global Reanalysis, vol. 146, pp. 1999–2049. https://doi.org/10.1002/qj.3803.
Hooyberghs, J., Mensink, C., Dumont, G., Fierens, F., Brasseur, O., 2005. A neural network forecast for daily average PM_{10} concentrations in Belgium. Atmos. Environ. 39, 3279–3289. https://doi.org/10.1016/j.atmosenv.2005.01.050.
Huang, J., Jaeglé, L., Chen, Q., Alexander, B., Sherwen, T., Evans, M.J., Theys, N., Choi, S., 2020. Evaluating the impact of blowing-snow sea salt aerosol on springtime BrO and O3 in the Arctic. Atmos. Chem. Phys. 20, 7335–7358. https://doi.org/10.5194/acp-20-7335-2020.
IPCC, 2021. In: Masson-Delmotte, V., Zhai, P., Pirani, A., Connors, S.L., Péan, C., Berger, S., Caud, N., Chen, Y., Goldfarb, L., Gomis, M.I., Huang, M., Leitzell, K., Lonnoy, E., Matthews, J.B.R., Maycock, T.K., Waterfield, T., Yelekçi, O., Yu, R., Zhou, B. (Eds.), Climate Change 2021: the Physical Science Basis. Contribution of Working Group I to the Sixth Assessment Report of the Intergovernmental Panel on Climate Change. Cambridge University Press (in press).
Jacobi, H.-W., Kaleschke, L., Richter, A., Rozanov, A., Burrows, J.P., 2006. Observation of a fast ozone loss in the marginal ice zone of the Arctic Ocean. J. Geophys. Res. Atmos. 111 https://doi.org/10.1029/2005JD006715.
Jones, A.E., Anderson, P.S., Begoin, M., Brough, N., Hutterli, M.A., Marshall, G.J., Richter, A., Roscoe, H.K., Wolff, E.W., 2009. BrO, blizzards, and drivers of polar tropospheric ozone depletion events. Atmos. Chem. Phys. 9, 4639–4652. https://doi.org/10.5194/acp-9-4639-2009.
Jones, A.E., Anderson, P.S., Wolff, E.W., Roscoe, H.K., Marshall, G.J., Richter, A., Brough, N., Colwell, S.R., 2010. Vertical structure of Antarctic tropospheric ozone depletion events: characteristics and broader implications. Atmos. Chem. Phys. 10, 7775–7794. https://doi.org/10.5194/acp-10-7775-2010.
Kaleschke, L., Richter, A., Burrows, J., Afe, O., Heygster, G., Notholt, J., Rankin, A.M., Roscoe, H.K., Hollwedel, J., Wagner, T., Jacobi, H.-W., 2004. Frost flowers on sea ice as a source of sea salt and their influence on tropospheric halogen chemistry. Geophys. Res. Lett. 31 https://doi.org/10.1029/2004GL020655.
Koop, T., Kapilashrami, A., Molina, L.T., Molina, M.J., 2000. Phase transitions of sea-salt/water mixtures at low temperatures: implications for ozone chemistry in the polar marine boundary layer. J. Geophys. Res. Atmos. 105, 26393–26402. https://doi.org/10.1029/2000JD900413.
Kreher, K., Johnston, P.V., Wood, S.W., Nardi, B., Platt, U., 1997. Ground-based measurements of tropospheric and stratospheric BrO at Arrival Heights, Antarctica. Geophys. Res. Lett. 24, 3021–3024. https://doi.org/10.1029/97GL02997.
Lieb-Lappen, R.M., Obbard, R.W., 2015. The role of blowing snow in the activation of bromine over first-year Antarctic sea ice. Atmos. Chem. Phys. 15, 7537–7545. https://doi.org/10.5194/acp-15-7537-2015.
Lu, J.Y., Schroeder, W.H., Barrie, L.A., Steffen, A., Welch, H.E., Martin, K., Lockhart, L., Hunt, R.V., Boila, G., Richter, A., 2001. Magnification of atmospheric mercury deposition to polar regions in springtime: the link to tropospheric ozone depletion chemistry. Geophys. Res. Lett. 28, 3219–3222. https://doi.org/10.1029/2000GL012603.
Masters, T., 1993. Practical Neural Network Recipes in C++. Morgan Kaufmann, p. 516. https://doi.org/10.1016/C2009-0-22399-3.
Müller, M.D., Kaifel, A., Weber, M., Burrows, J.P., 2002. Neural network scheme for the retrieval of total ozone from Global Ozone Monitoring Experiment data. Appl. Opt. 41, 5051–5058. https://doi.org/10.1364/AO.41.005051.
Nicely, J.M., Duncan, B.N., Hanisco, T.F., Wolfe, G.M., Salawitch, R.J., Deushi, M., Haslerud, A.S., Jöckel, P., Josse, B., Kinnison, D.E., Klekociuk, A., Manyin, M.E., Marécal, V., Morgenstern, O., Murray, L.T., Myhre, G., Oman, L.D., Pitari, G., Pozzer, A., Quaglia, I., Revell, L.E., Rozanov, E., Stenke, A., Stone, K., Strahan, S., Tilmes, S., Tost, H., Westervelt, D.M., Zeng, G., 2020. A machine learning examination of hydroxyl radical differences among model simulations for CCMI-1. Atmos. Chem. Phys. 20, 1341–1361. https://doi.org/10.5194/acp-20-1341-2020.
Peterson, P.K., Hartwig, M., May, N.W., Schwartz, E., Rigor, I., Ermold, W., Steele, M., Morison, J.H., Nghiem, S.V., Pratt, K.A., 2019. Snowpack measurements suggest role for multi-year sea ice regions in Arctic atmospheric bromine and chlorine chemistry. Elementa: SSci. Anthropocene 7, 14. https://doi.org/10.1525/elementa.352.
Peterson, P.K., Pöhler, D., Sihler, H., Zielcke, J., General, S., Frieß, U., Platt, U., Simpson, W.R., Nghiem, S.V., Shepson, P.B., Stirm, B.H., Dhaniyala, S., Wagner, T., Caulton, D.R., Fuentes, J.D., Pratt, K.A., 2017. Observations of bromine monoxide transport in the Arctic sustained on aerosol particles. Atmos. Chem. Phys. 17, 7567–7579. https://doi.org/10.5194/acp-17-7567-2017.
Platt, U., Perner, D., 1983. Measurements of atmospheric trace gases by long path differential UV/visible absorption spectroscopy. In: Killinger, D.K., Mooradian, A. (Eds.), Optical and Laser Remote Sensing. Springer, Berlin, Heidelberg, pp. 97–105. https://doi.org/10.1007/978-3-540-39552-2_13.
Platt, U., Wagner, T., 1998. Satellite mapping of enhanced BrO concentrations in the troposphere. Nature 395, 486–490. https://doi.org/10.1038/26723.
Rasp, S., Lerch, S., 2018. Neural networks for postprocessing ensemble weather forecasts. Mon. Weather Rev. 146, 3885–3900. https://doi.org/10.1175/MWR-D-18-0187.1.
Richter, A., Wittrock, F., Eisinger, M., Burrows, J.P., 1998. GOME observations of tropospheric BrO in northern hemispheric spring and summer 1997. Geophys. Res. Lett. 25, 2683–2686. https://doi.org/10.1029/98GL52016.
Roscoe, H.K., Brough, N., Jones, A.E., Wittrock, F., Richter, A., Van Roozendael, M., Hendrick, F., 2014. Characterisation of vertical BrO distribution during events of enhanced tropospheric BrO in Antarctica, from combined remote and in-situ measurements. J. Quant. Spectrosc. Radiat. Transf. 138, 70–81. https://doi.org/10.1016/j.jqsrt.2014.01.026.
Rozanov, A., Rozanov, V., Buchwitz, M., Kokhanovsky, A., Burrows, J.P., 2005. SCIATRAN 2.0 – a new radiative transfer model for geophysical applications in the 175–2400nm spectral region. Adv. Space Res. 36, 1015–1019. https://doi.org/10.1016/j.asr.2005.03.012.
Salawitch, R.J., Canty, T., Kurosu, T., Chance, K., Liang, Q., Silva, A. da, Pawson, S., Nielsen, J.E., Rodriguez, J.M., Bhartia, P.K., Liu, X., Huey, L.G., Liao, J., Stickel, R.E., Tanner, D.J., Dibb, J.E., Simpson, W.R., Donohoue, D., Weinheimer, A., Flocke, F., Knapp, D., Montzka, D., Neuman, J.A., Nowak, J.B., Ryerson, T.B., Oltmans, S., Blake, D.R., Atlas, E.L., Kinnison, D.E., Tilmes, S., Pan, L.L., Hendrick, F., Roozendael, M.V., Kreher, K., Johnston, P.V., Gao, R.S., Johnson, B., Bui, T.P., Chen, G., Pierce, R.B., Crawford, J.H., Jacob, D.J., 2010. A new interpretation of total column BrO during Arctic spring. Geophys. Res. Lett. 37 https://doi.org/10.1029/2010GL043798.
Sander, R., Burrows, J., Kaleschke, L., 2006. Carbonate precipitation in brine ? a potential trigger for tropospheric ozone depletion events. Atmos. Chem. Phys. 6, 4653–4658.
Seo, S., Richter, A., Blechschmidt, A.-M., Bougoudis, I., Burrows, J.P., 2019. First high-resolution BrO column retrievals from TROPOMI. Atmos. Meas. Tech. 12, 2913–2932. https://doi.org/10.5194/amt-12-2913-2019.
Seo, S., Richter, A., Blechschmidt, A.-M., Bougoudis, I., Burrows, J.P., 2020. Spatial distribution of enhanced BrO and its relation to meteorological parameters in Arctic and Antarctic sea ice regions. Atmos. Chem. Phys. 20, 12285–12312. https://doi.org/10.5194/acp-20-12285-2020.
Serreze, M.C., Barrett, A.P., 2010. Characteristics of the Beaufort Sea high. J. Clim. 24, 159–182. https://doi.org/10.1175/2010JCLI3636.1.
Serreze, M.C., Barry, R.G., 2011. Processes and impacts of Arctic amplification: a research synthesis. Global Planet. Change 77, 85–96. https://doi.org/10.1016/j.gloplacha.2011.03.004.
Simpson, W.R., Carlson, D., Hönninger, G., Douglas, T.A., Sturm, M., Perovich, D., Platt, U., 2007. First-year sea-ice contact predicts bromine monoxide (BrO) levels at Barrow, Alaska better than potential frost flower contact. Atmos. Chem. Phys. 7, 621–627.
Stathakis, D., 2009. How many hidden layers and nodes? Int. J. Rem. Sens. 30, 2133–2147. https://doi.org/10.1080/01431160802549278.
Theys, N., Roozendael, M.V., Errera, Q., Hendrick, F., Daerden, F., Chabrillat, S., Dorf, M., Pfeilsticker, K., Rozanov, A., Lotz, W., Burrows, J.P., Lambert, J.-C., Goutail, F., Roscoe, H.K., Mazière, M.D., 2009. A global stratospheric bromine monoxide climatology based on the BASCOE chemical transport model. Atmos. Chem. Phys. 9, 831–848. https://doi.org/10.5194/acp-9-831-2009.
Toohey, D.W., Anderson, J.G., Brune, W.H., Chan, K.R., 1990. In situ measurements of BrO in the Arctic stratosphere. Geophys. Res. Lett. 17, 513–516. https://doi.org/10.1029/GL017i004p00513.
Tschudi, M., Meier, W.N., Stewart, J.S., Fowler, C., Maslanik, J., 2019. EASE-Grid Sea Ice Age, Version 4. [1996-2017]. Boulder, Colorado USA. NASA National Snow and Ice Data Center Distributed Active Archive Center. https://doi.org/10.5067/UTAV7490FEPB.
Tuckermann, M., Ackermann, R., Golz, C., Lorenzen-Schmidt, H., Senne, T., Stutz, J., Trost, B., Unold, W., Platt, U., 1997. DOAS-observation of halogen radical-catalysed arctic boundary layer ozone destruction during the ARCTOC-campaigns 1995 and 1996 in Ny-Alesund. Spitsbergen, Tellus B 49, 533–555. https://doi.org/10.1034/j.1600-0889.49.issue5.9.x.
Van Roozendael, M., Wagner, T., Richter, A., Pundt, I., Arlander, D.W., Burrows, J.P., Chipperfield, M., Fayt, C., Johnston, P.V., Lambert, J.-C., Kreher, K., Pfeilsticker, K., Platt, U., Pommereau, J.-P., Sinnhuber, B.-M., Tørnkvist, K.K., Wittrock, F., 2002. Intercomparison of BrO measurements from ERS-2 GOME, ground-based and balloon platforms. Adv. Space Res. 29, 1661–1666. https://doi.org/10.1016/S0273-1177(02)00098-4.
Wagner, T., Leue, C., Wenig, M., Pfeilsticker, K., Platt, U., 2001. Spatial and temporal distribution of enhanced boundary layer BrO concentrations measured by the GOME instrument aboard ERS-2. J. Geophys. Res. Atmos. 106, 24225–24235. https://doi.org/10.1029/2000JD000201.
Wang, S.-C., 2003. Artificial neural network. In: Interdisciplinary Computing in Java Programming. Springer US, Boston, MA, pp. 81–100. https://doi.org/10.1007/978-1-4615-0377-4_5.
Warsito, B., Santoso, R., Suparti, Yasin, H., 2018. Cascade forward neural network for time series prediction. J. Phys.: Conf. Ser. 1025, 012097 https://doi.org/10.1088/1742-6596/1025/1/012097.
Yang, X., Blechschmidt, A.-M., Bognar, K., McClure-Begley, A., Morris, S., Petropavlovskikh, I., Richter, A., Skov, H., Strong, K., Tarasick, D.W., Uttal, T., Vestenius, M., Zhao, X., 2020. Pan-Arctic surface ozone: modelling vs. measurements. Atmos. Chem. Phys. 20, 15937–15967. https://doi.org/10.5194/acp-20-15937-2020.
Zurada, J.M., 1992. Introduction to Artificial Neural Systems. West Publishing Company, New York. https://dl.acm.org/doi/10.5555/131393.